CIRCULAR AUXETIC PLATES

T.-C. Lim *

School of Science and Technology
SIM University
S 599491, Republic of Singapore

ABSTRACT

This paper investigates the suitability of auxetic materials for load-bearing circular plates. It is herein shown that the optimal Poisson's ratio for minimizing the bending stresses is strongly dependent on the final deformed shape, load distribution, and the type of edge supports. Specifically, the use of auxetic material for circular plates is recommended when (a) the plate is bent into a spherical or spherical-like cap, (b) a point load is applied to the center of the plate regardless of the edge conditions, and (c) a uniform load is applied on a simply-supported plate. However, auxetic materials are disadvantaged when a flat plate is to be bent into a saddle-like shell. The optimal Poisson's ratios concept recommended in this paper is useful for providing an added design consideration. In most cases, the use of auxetic materials for laterally loaded circular plates is more advantageous compared to the use of materials with conventional Poisson's ratio, with other factors fixed. This is achieved through materials-based stress redistribution in addition to the common practices of dimensioning-based stress redistribution and materials strengthening.

Keywords: Auxetic materials, Circular plates, Mechanical properties.

1. INTRODUCTION

Auxetic materials are solids that possess negative Poisson's ratio, *i.e.* they expand and contract transversely when stretched or compressed, respectively, in the longitudinal direction. As a result, auxetic plates undergo synclastic deformation when bending moments are applied on two opposing sides, instead of anticlastic deformation in the case of conventional plates. It follows that when a circular plate is laterally loaded such that its deformation approximates the surface of a sphere, the bending moment, and hence the bending stresses, are reduced by the auxeticity of the plate material. Various forms of auxetic materials have been developed, observed or modeled, including ferromagnetic films [1], FCC crystals [2], hexagonal molecules in 2D lattice [3,4] and foams [5-8]. The counter intuitive nature of auxetic materials avails much potential as safer fasteners [9], improved arterial prostheses [10], artificial intervertebral disc [11], drug eluting stents [12] and other prostheses [13], more comfortable cushions [14,15], highly tunable molecular sieve [16-19], antivibration glove [20], novel textiles [21], better material for diabetic shoes [22], safer pressure vessels [23] and other thin walled structures [24], and higher performing crash/shock absorber [25,26], to name a few. Theoretical models have been proposed to elucidate such counter intuitive behavior while experimental validation have been carried out to understand this behavior from the microstructural standpoint [27-37]. Recently, research in auxetic materials extends to the unique structural properties of auxetic plates as a result of their material behavior. These include sandwich plates [38,39] and thermoelastic layered plates [40], strain energy distribution in an auxetic plate with a crack [41], finite element analysis of auxetic plate deformation in 3D [42] and 2D [43], as well as solitary waves in auxetic plates [44].

Although it is known in the literature that that auxetic materials can reduce stress in plate bending problem, no quantitative study has been made. In this paper, axisymmetric bending a circular plate is considered to quantitatively study the extent of stress reduction when the Poisson's ratio of the plate material changes from a positive value to a negative value. Where applicable, the optimal Poisson's ratio of a circular plate is obtained under specific loading condition (s) with other material parameters fixed.

2. EFFECT OF AUXETICITY ON TYPES OF BENT SHAPE

With reference to Fig. 1, the radial and tangential moments per unit length, M_r and M_t, of a circular plate is related to the Poisson's ratio, v, and the deflection w at a radial distance of r from the plate center are given by [45-48]

* Corresponding author (alan_tc_lim@yahoo.com)

DOI : 10.1017/jmech.2012.113
Copyright © 2013 The Society of Theoretical and Applied Mechanics, R.O.C.
https://doi.org/10.1017/jmech.2012.113 Published online by Cambridge University Press

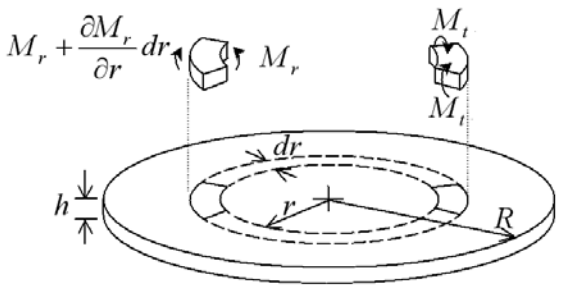


Fig. 1 A schematic of the bending moments

$$M_r = -D\left(\frac{d^2w}{dr^2} + \frac{v}{r}\frac{dw}{dr}\right) \tag{1}$$

$$M_t = -D\left(\frac{1}{r}\frac{dw}{dr} + v\frac{d^2w}{dr^2}\right) \tag{2}$$

with the bending stiffness of the plate, D, being

$$D = \frac{Eh^3}{12(1-v^2)} \tag{3}$$

where by E and h are the Young's modulus and thickness of the plate respectively.

The maximum bending stresses occur at the lower and upper surfaces of the plate, and are given by

$$\begin{Bmatrix}\sigma_r \\ \sigma_t\end{Bmatrix}_{\max} = \pm\frac{6}{h^2}\begin{Bmatrix}M_r \\ M_t\end{Bmatrix}, \tag{4}$$

there by implying that the bending moments must be reduced if the bending stresses are to be reduced. Employing the Cartesian coordinate system, the bending stresses can be written as

$$\begin{Bmatrix}\sigma_x \\ \sigma_y\end{Bmatrix} = \frac{Ez}{1-v^2}\begin{bmatrix}1 & v \\ v & 1\end{bmatrix}\begin{Bmatrix}r_x^{-1} \\ r_y^{-1}\end{Bmatrix}, \tag{5}$$

where r_x and r_y denote the radius of curvature of the plate's neutral surface in sections parallel to the xz and yz planes respectively. Consequently, the optimal Poisson's ratio of the plate material is

$$v_{\text{opt}} = -\frac{r_y}{r_x} \Leftrightarrow \sigma_x = (\sigma_x)_{\min} \tag{6}$$

for minimizing the bending stress σ_x. It can be seen from Eqs. (5) and (6) that if the plate is to be bent into a spherical shell (*i.e.* $r_x = r_y$), then the bending stresses σ_x and σ_y are minimized when the plate is auxetic with $v = -1$. Reference to Eq. (6) suggests that if the plate is to be bent into a cylindrical shell such that $r_x \to \infty$, then the bending stress σ_x is minimized when $v = 0$. Going by the same reasoning, if the plate is to be bent into a saddle-like shell whereby $r_x = -2r_y$ (the negative sign denoting the radius of curvatures being on opposite sides of the bent plate), then the bending stress σ_x is minimized when the plate is non-auxetic with $v = 0.5$.

3. EFFECT OF AUXETICITY ON UNIFORMLY LOADED CIRCULAR PLATES

The radial and tangential bending moments per unit length for a uniformly loaded circular plate with built in edge are given as [45-48]

$$\begin{Bmatrix}M_r \\ M_t\end{Bmatrix} = \frac{q}{16}\begin{bmatrix}1+v & 3+v \\ 1+v & 1+3v\end{bmatrix}\begin{Bmatrix}+R^2 \\ -r^2\end{Bmatrix} \tag{7}$$

where R is the radius of the circular plate and q is the load intensity in force per unit area. Adopting dimensionless parameters

$$M^* = \frac{16}{qR^2}M \tag{8}$$

and (r/R), we have

$$\begin{Bmatrix}M_r^* \\ M_t^*\end{Bmatrix} = (1+v)\begin{bmatrix}1 & \left(\frac{3+v}{1+v}\right) \\ 1 & \left(\frac{1+3v}{1+v}\right)\end{bmatrix}\begin{Bmatrix}1 \\ -(r/R)^2\end{Bmatrix}. \tag{9}$$

It is quite sufficient to adopt the radial and tangential bending moments, or their dimensionless forms, because any non-dimensionalization of the maximum radial and tangential bending stresses will lead to an expression similar to Eq. (9). This is because introducing the dimensionless parameter for stress

$$\sigma^{(*)} = \frac{8\sigma}{3q}\left(\frac{h}{R}\right)^2 \tag{10}$$

gives the maximum dimensionless bending stresses

$$\begin{Bmatrix}\sigma_r^{(*)} \\ \sigma_t^{(*)}\end{Bmatrix}_{\max} = \frac{8\sigma}{3q}\left(\frac{h}{R}\right)^2\begin{Bmatrix}\sigma_r \\ \sigma_t\end{Bmatrix}_{\max} = (1+v)\begin{bmatrix}1 & \left(\frac{3+v}{1+v}\right) \\ 1 & \left(\frac{1+3v}{1+v}\right)\end{bmatrix}\begin{Bmatrix}1 \\ -(r/R)^2\end{Bmatrix}, \tag{11}$$

which is similar to Eq. (9). Nevertheless the dimensionless parameter for stress is useful for non- dimensionlizing the effective stress

$$\sigma_{\text{eff}} = \frac{1}{\sqrt{2}}\sqrt{(\sigma_r-\sigma_t)^2 + (\sigma_t-\sigma_z)^2 + (\sigma_z-\sigma_r)^2 + 6(\tau_{tz}^2 + \tau_{zr}^2 + \tau_{rt}^2)}. \tag{12}$$

Since bending stresses are the largest at a distance furthest from the middle surface of the plate, *i.e.* at the surface, it is useful to note that $\sigma_z = 0$ on the surface that is not loaded, while $\sigma_z = -q$ on the loaded surface. For the latter, $|\sigma_z| = q << (\sigma_r)_{\max}, (\sigma_t)_{\max}$. The in-plane shear stress τ_{rt} and one of the two out-of-plane

https://doi.org/10.1017/jmech.2012.113 Published online by Cambridge University Press

shear stresses τ_{tz} are zero for the chosen elemental volumes aligned in the direction shown in Fig. 1. The other out-of-plane shear stress, $\tau_{tr} = \tau_{rt}$ follows a parabolic distribution along the thickness of the plate such that it is zero at the surface and takes its maximum value at the middle plane of the plate. This reduces Eq. (12) to

$$\sigma_{\text{eff}} = \sqrt{\sigma_r^2 + \sigma_t^2 - \sigma_r \sigma_t} \ . \tag{13}$$

Based on Eqs. (4) and (7), we have the effective stress distribution

$$\sigma_{\text{eff}} = \frac{3qR^2}{8h^2}\sqrt{(1+\nu)^2\left[1-4\left(\frac{r}{R}\right)^2\right]+(7+2\nu+7\nu^2)\left(\frac{r}{R}\right)^4} \tag{14}$$

or its dimensionless form

$$\sigma_{\text{eff}}^{(*)} = \sqrt{(1+\nu)^2\left[1-4\left(\frac{r}{R}\right)^2\right]+(7+2\nu+7\nu^2)\left(\frac{r}{R}\right)^4} \tag{15}$$

by virtue of Eq. (10).

For a uniformly loaded plate supported at its edge, the maximum shearing stress is at the middle surface of the plate (*i.e.* at the neutral axis in which the bending stresses are zero) and at a radial distance furthest from the plate axis

$$(\tau_{rt})_{\max} = \frac{3qr}{4h} = \frac{3qR}{4h}\left(\frac{r}{R}\right) \tag{16}$$

considering parabolic distribution along the thickness of the plate. One may compare this with the bending stresses at the surface of the plate

$$\begin{Bmatrix}\sigma_r \\ \sigma_t\end{Bmatrix}_{\max} = \pm\frac{3qR^2}{8h^2}\begin{bmatrix}(1+\nu) & (3+\nu) \\ (1+\nu) & (1+3\nu)\end{bmatrix}\begin{Bmatrix}1 \\ -(r/R)^2\end{Bmatrix} . \tag{17}$$

Since $R >> h$, the maximum shear stress at the middle plane of the plate is generally lower than the bending stresses at the surface of the plate

$$\frac{(\tau_{rt})_{\max}}{(\sigma)_{\max}} \approx \frac{\left(\frac{3qR}{4h}\right)}{\left(\frac{3qR^2}{8h^2}\right)} = \frac{2h}{R} \ . \tag{18}$$

As such the effective stress is adopted at the surface rather than at the mid-plane due to the greater maximum bending stress at the surface (with zero out-of-plane shear) than the maximum shear stress at the mid-plane (with zero bending stress).

The plate deflection

$$w = \frac{q}{64D}(R^2 - r^2)^2 \tag{19}$$

is maximum at the center

$$w_{\max} = \frac{qR^4}{64D} \ . \tag{20}$$

Although the maximum deflection appears to be independent from the Poisson's ratio of the plate, it is not so. The Poisson's ratio dependency is due to the fact that the plate bending stiffness

$$D = \frac{Eh^3}{12(1-\nu^2)} \tag{21}$$

is influenced by the Poisson's ratio of the plate material. Substituting the plate stiffness expression into the maximum plate deflection description, we have

$$w_{\max} = \frac{3qR^4}{16h^3E}(1-\nu^2) \ . \tag{22}$$

Bearing in mind the moduli relation

$$G = \frac{E}{2(1+\nu)} \tag{23}$$

for an isotropic material, the maximum plate deflection can also be written as

$$w_{\max} = \frac{3qR^4}{16h^3G}\left(\frac{1-\nu}{2}\right) \ . \tag{24}$$

This implies that a change in the Poisson's ratio of any material is accompanied by a change in the Young's modulus at constant shear modulus or a change in the shear modulus at constant Young's modulus. These are extreme cases, as both moduli may change simultaneously. Taking square root of the product of both maximum deflections give rise to

$$w_{\max} = \frac{3qR^4}{16h^3\sqrt{EG}}(1-\nu)\sqrt{\frac{1+\nu}{2}} \ . \tag{25}$$

This maximum deflection description allows both moduli to change simultaneously to the change in Poisson's ratio, with the condition that the product of both moduli remains constant. For investigating only the effect of Poisson's ratio on the maximum plate deflection, it is useful to introduce the following dimensionless parameters

$$w_{\max}^{(E*)} = \frac{16w_{\max}\,h^3E}{3qR^4} \ , \tag{26}$$

$$w_{\max}^{(G*)} = \frac{16w_{\max}\,h^3G}{3qR^4} \tag{27}$$

and

$$w_{\max}^{(\sqrt{EG}*)} = \frac{16w_{\max}\,h^3\sqrt{EG}}{3qR^4} \tag{28}$$

so that the following dimensionless parameters

https://doi.org/10.1017/jmech.2012.113 Published online by Cambridge University Press

$$w_{\max}^{(E*)} = 1 - \nu^2 \ , \tag{29}$$

$$w_{\max}^{(G*)} = \frac{1-\nu}{2} \tag{30}$$

and

$$w_{\max}^{(\sqrt{EG}*)} = (1-\nu)\sqrt{\frac{1+\nu}{2}} \tag{31}$$

describe the maximum plate deflection on the basis of constant Young's modulus, constant shear modulus, and constant product of both moduli respectively, as the plate material changes in its Poisson's ratio.

Figures 2(a) and 2(b) show the plots of dimensionless bending moments and dimensionless effective stress versus dimensionless radius for a fully-clamped circular plate under uniform load, while Fig. 2(c) illustrates the change in the dimensionless maximum deflection with auxeticity of the plate material.

The plotted results in Fig. 2(a) show that the largest bending moment, and hence the largest bending stress, occurs at the edge of the plate whereby the dimensionless radial bending moment, $\left|M_r^*\right|_{r=R} = 2$, is independent from the Poisson's ratio of the plate. The dimensionless tangential bending moment at the edge generally possesses lower magnitude than the dimensionless radial bending moment, with an exception when the plate's Poisson's ratio is $\nu = -1$, which gives $\left|M_r^*\right|_{r=R} = \left|M_t^*\right|_{r=R}$ at the plate edge. Using bending moment as a physical quantity under the conditions of uniform load and built-in edge, a comparison of bending stresses at the boundary can be made, *i.e.* $(M_r)_{r=R} > (M_t)_{r=R}$ or $|\sigma_r|_{r=R,z=\pm h/2} = 0.75q(R/h)^2 > 0.75\nu q(R/h)^2 = |\sigma_t|_{r=R,z=\pm h/2}$ for $-1 < \nu \le 0.5$ and $(M_r)_{r=R} = (M_t)_{r=R}$ or $|\sigma_r|_{r=R,z=\pm h/2} = 0.75q(R/h)^2 = |\sigma_t|_{r=R,z=\pm h/2}$ for $\nu = -1$. This means that under the condition of uniformly distributed load, the maximum bending stresses at built-in edge in no longer confined only to the radial direction, but also includes the tangential direction if the plate material is highly auxetic at $\nu = -1$. Two further points are of interest: (i) the tangential bending moment, and hence the tangential bending stress, is zero at the plate edge if the plate material's Poisson's ratio is $\nu = 0$, and (ii) the bending moment, and hence the bending stresses, at the plate center is zero as the Poisson's ratio of the plate material approaches $\nu = -1$. Figure 2(b) shows that, on the basis of effective stress, the use of auxetic materials for uniformly loaded circular plates is not suitable if the edge is fully clamped, as auxeticity tends to shift the distribution of effective stress to the plate rim. Figure 2(c) illustrates the effect of Poisson's ratio on the maximum deflection of the plate. In particular, deflection is can be effectively reduced either by using highly auxetic material (*e.g.* $\nu = -1$) at fixed Young's modulus or at fixed moduli product, or by using a high Poisson's ratio material (*e.g.* $\nu = 0.5$) at fixed shear modulus.

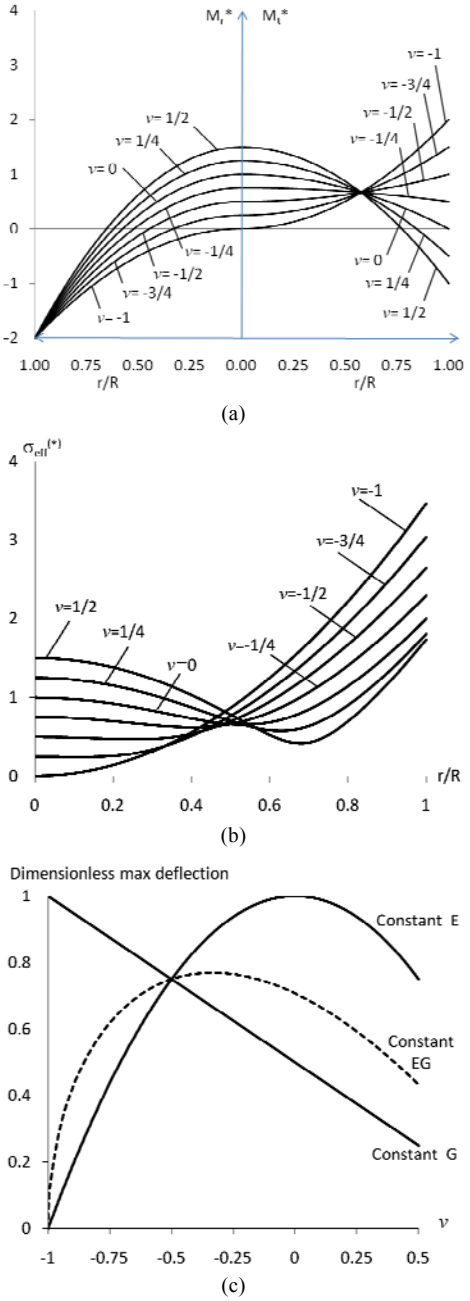


Fig. 2 A fully-clamped circular plate under uniform load: (a) dimensionless bending moment distributions, (b) dimensionless effective stress distributions, and (c) dimensionless maximum deflection

The bending moments for a uniformly loaded circular plate with simply-supported edge are given as [45-48]

$$\begin{Bmatrix} M_r \\ M_t \end{Bmatrix} = \frac{q}{16}\begin{bmatrix} 3+\nu & 3+\nu \\ 3+\nu & 1+3\nu \end{bmatrix}\begin{Bmatrix} +R^2 \\ -r^2 \end{Bmatrix} \tag{32}$$

or, in dimensionless terms,

$$\begin{Bmatrix} M_r^* \\ M_t^* \end{Bmatrix} = (3+\nu)\begin{bmatrix} 1 & 1 \\ 1 & \left(\dfrac{1+3\nu}{3+\nu}\right) \end{bmatrix}\begin{Bmatrix} 1 \\ -(r/R)^2 \end{Bmatrix} . \tag{33}$$

https://doi.org/10.1017/jmech.2012.113 Published online by Cambridge University Press

Substituting Eq. (32) into Eq. (4) and using the dimensionless stress parameter described by Eq. (10), the effective stress of Eq. (13) is written as

$$\sigma_{\text{eff}} = \frac{3qR^2}{8h^2}\sqrt{(3+\nu)\left[(3+\nu)-4(1+\nu)\left(\frac{r}{R}\right)^2\right]+(7+2\nu+7\nu^2)\left(\frac{r}{R}\right)^4} \tag{34}$$

or in its dimensionless form as

$$\sigma_{\text{eff}}^{(*)} = \sqrt{(3+\nu)\left[(3+\nu)-4(1+\nu)\left(\frac{r}{R}\right)^2\right]+(7+2\nu+7\nu^2)\left(\frac{r}{R}\right)^4} \,. \tag{35}$$

The plate deflection

$$w = \frac{q(R^2-r^2)}{64D}\left(\frac{5+\nu}{1+\nu}R^2-r^2\right) \tag{36}$$

is maximum at the center

$$w_{\max} = \frac{qR^4}{64D}\left(\frac{5+\nu}{1+\nu}\right). \tag{37}$$

Substituting the plate bending stiffness expression into the maximum plate deflection, we have

$$w_{\max} = \frac{3qR^4}{16h^3E}(5+\nu)(1-\nu) \tag{38}$$

or, by using Eq. (23),

$$w_{\max} = \frac{3qR^4}{16h^3G}\frac{(5+\nu)(1-\nu)}{2(1+\nu)} \,. \tag{39}$$

Taking square root of the product of both maximum deflections give rise to

$$w_{\max} = \frac{3qR^4}{16h^3\sqrt{EG}}\frac{(5+\nu)(1-\nu)}{\sqrt{2(1+\nu)}} \,. \tag{40}$$

Using the dimensionless parameters described in Eqs. (26) to (28), the following dimensionless maximum deflections are obtained

$$w_{\max}^{(E*)} = (5+\nu)(1-\nu) \,, \tag{41}$$

$$w_{\max}^{(G*)} = \frac{(5+\nu)(1-\nu)}{2(1+\nu)} \tag{42}$$

and

$$w_{\max}^{(\sqrt{EG}*)} = \frac{(5+\nu)(1-\nu)}{\sqrt{2(1+\nu)}} \tag{43}$$

for quantifying the maximum plate deflection on the basis of constant Young's modulus, constant shear modulus, and constant product of both moduli, as the plate material changes in its Poisson's ratio.

Figures 3(a) and 3(b) outline the plots of dimensionless bending moments and dimensionless effective stress versus dimensionless radius for a simply-supported circular plate under uniform load, while Fig. 3(c) shows the variation in the dimensionless maximum deflection with auxeticity of the plate material.

It is known that, as a result free surface associated with simple supports, the radial bending moment is zero at the plate's edge. Plotted results in Fig. 3(a) further reveal that the bending moments, and hence the bending stresses, at the center of the plate reduce as the plate material's Poisson's ratio reduces from $\nu = 0.5$

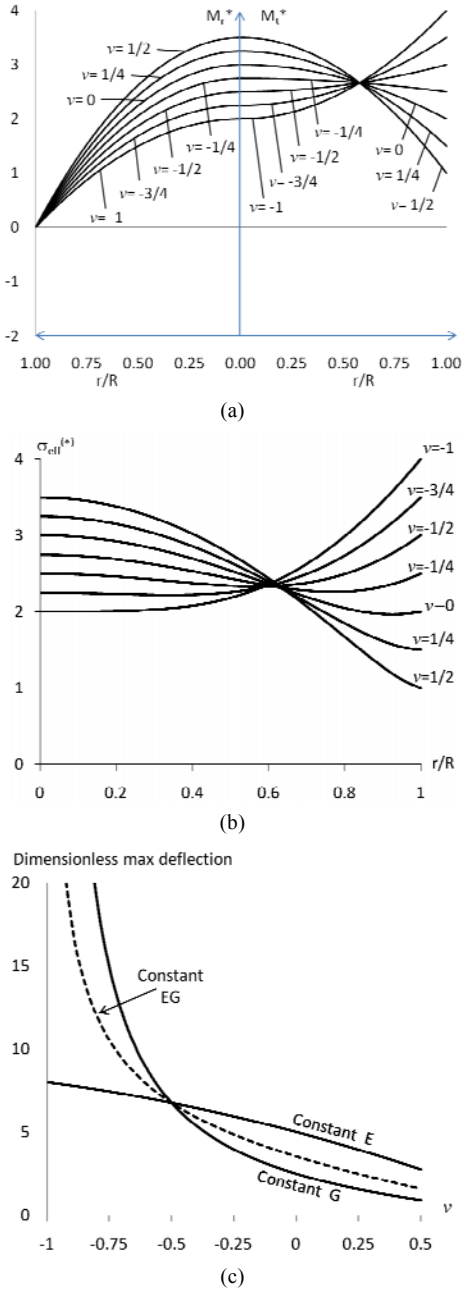


Fig. 3 A simply-supported circular plate under uniform load: (a) dimensionless bending moment distributions, (b) dimensionless effective stress distributions, and (c) dimensionless maximum deflection

https://doi.org/10.1017/jmech.2012.113 Published online by Cambridge University Press

to $v=-1$. While the tangential bending moment at the plate center decreases with decreasing Poisson's ratio, an opposite effect occurs at the edge of the plate. This suggests that the maximum tangential bending stress that takes place at the plate center at v = 0.5 reduces with the Poison's ratio until a negative Poisson's ratio is attained. Thereafter, the maximum tangential bending stress switches location to the plate rim. This maximum stress increases with decreasing Poisson's ratio of the plate material. Reference to Figs. 3(a) and 3(b) shows that an optimum plate Poisson's ratio, under uniform load with simply supported edge, falls between $v=-1/4$ and $v=-1/2$. With reference to Fig. 3(a), the optimal Poisson's ratio can be obtained by solving

$$\frac{dM_t^*}{d(r/R)}=0 \tag{44}$$

to give

$$v_{op}=-\frac{1}{3}\,. \tag{45}$$

A similar optimal Poisson's ratio can be obtained by reference to Fig. 3(b). In the latter, it can be seen that $\left(\sigma_{\text{eff}}^{(*)}\right)_{r=0}=\left(\sigma_{\text{eff}}^{(*)}\right)_{r=R}=8/3$ when the Poisson's ratio is $v=-1/3$. This is the optimal condition as $\left(\sigma_{\text{eff}}^{(*)}\right)_{r=0}>8/3$ for $v>-1/3$ and $\left(\sigma_{\text{eff}}^{(*)}\right)_{r=R}>8/3$ for $v<-1/3$. Figure 3(c) reveals that the maximum deflection is reduced when conventional materials, rather than auxetic ones are used. In particular, the use of highly auxetic material at constant shear modulus or at constant product of Young's and shear moduli leads to very large deflection. However, the use of highly auxetic material results in a very small increase to the plate deflection if the reduction of Poisson's ratio is accompanied by constant Young's modulus.

To appreciate the extent of maximum stress reduction with the use of the optimal Poisson's ratio $v_{opt}=-1/3$, a comparison is made with a plate of conventional Poisson's ratio of $v=+1/3$. Figure 4 shows the dimensionless bending moments and dimensionless effective stress plotted with respect to the dimensionless radius.

As evident from Fig. 4(a), the use of plate with Poisson's ratio $v=-1/3$ retains the dimensionless tangential bending moment, which is higher than the dimensionless radial bending moment, at $M_t^*=8/3$, which corresponds to $M_t = qR^2/6$ or $(\sigma_t)_{\max} = q(R/h)^2$, throughout the entire plate. On the other hand, the use of a plate with a conventional Poisson's ratio of $v=1/3$ gives the maximum dimensionless bending moment of $M_r^*=M_t^*=10/3$, which corresponds to $M_r = M_t = 1.25qR^2/6$ or $(\sigma_r)_{\max}=(\sigma_t)_{\max}= 1.25q(R/h)^2$ at the plate center. Similarly from Fig. 4(b), the maximum dimensionless effective stresses are $\sigma_{\text{eff}}^{(*)}=10/3$ and $\sigma_{\text{eff}}^{(*)}=8/3$ for $v=1/3$ and $v=-1/3$ respectively. The non-optimal use of simply-supported conventional circular plates under uniform loading leads to wastage as a result of the bending stress being not fully distributed. The change of plate material's Poisson's ratio from $v=1/3$ to $v=-1/3$ reduces the maximum bending stress by 20% via redistribution of the tangential bending moment.

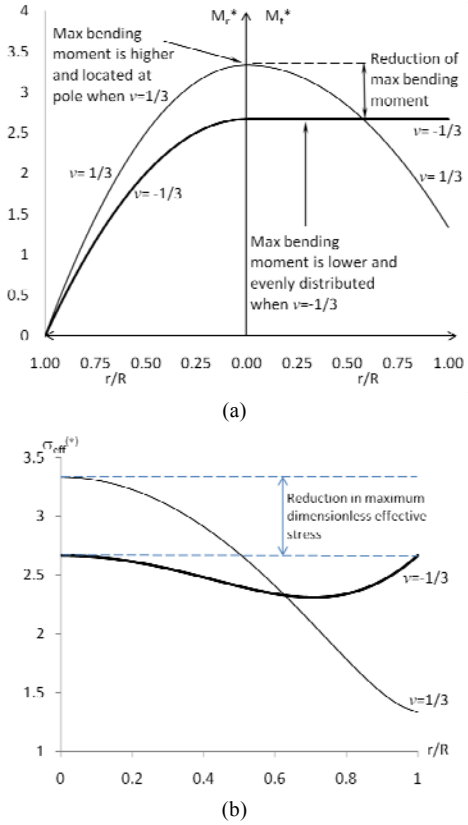


Fig. 4 (a) Dimensionless bending moment distributions, and (b) dimensionless effective stress distributions, for a uniformly loaded simply-supported circular plate with optimum Poisson's ratio ($v=-1/3$) and its corresponding conventional Poisson's ratio (v = 1/3)

4. EFFECT OF AUXETICITY ON CENTRALLY POINT-LOADED CIRCULAR PLATES

The bending moments for a circular plate with a point load P applied at the center of the plate that is clamped at the edge are given as [45-48]

$$\begin{Bmatrix} M_r \\ M_t \end{Bmatrix}=\frac{P}{4\pi}\begin{bmatrix} 1+v & 1 \\ 1+v & v \end{bmatrix}\begin{Bmatrix} \ln(R/r) \\ -1 \end{Bmatrix}. \tag{46}$$

Adopting another dimensionless parameter

$$M^{**}=\frac{4\pi}{P}M \tag{47}$$

and (r/R), Eq. (46) can be simplified to

$$\begin{Bmatrix} M_r^{**} \\ M_t^{**} \end{Bmatrix}=\begin{bmatrix} 1+v & 1 \\ 1+v & v \end{bmatrix}\begin{Bmatrix} \ln(R/r) \\ -1 \end{Bmatrix}. \tag{48}$$

https://doi.org/10.1017/jmech.2012.113 Published online by Cambridge University Press

Substituting Eq. (46) into Eq. (4) and using the dimensionless stress parameter

$$\sigma^{(**)} = \frac{2\pi h^2 \sigma}{3P} , \tag{49}$$

the effective stress of Eq. (13) can be written as

$$\sigma_{\text{eff}} = \frac{3P}{2\pi h^2}\sqrt{(1+v)^2 \ln\left(\frac{R}{r}\right)\left[\ln\left(\frac{R}{r}\right)-1\right]+1+v+v^2} \tag{50}$$

or in its dimensionless form as

$$\sigma_{\text{eff}}^{(**)} = \sqrt{(1+v)^2 \ln\left(\frac{R}{r}\right)\left[\ln\left(\frac{R}{r}\right)-1\right]+1+v+v^2} . \tag{51}$$

The plate deflection

$$w = \frac{Pr^2}{8\pi D}\ln\left(\frac{r}{R}\right)+\frac{P}{16\pi D}(R^2-r^2) \tag{52}$$

is maximum at the center

$$w_{\max} = \frac{PR^2}{16\pi D} . \tag{53}$$

Substituting the plate bending stiffness expression into the maximum plate deflection, we have

$$w_{\max} = \frac{3PR^2}{4\pi h^3 E}(1-v^2) \tag{54}$$

or, by using Eq. (23),

$$w_{\max} = \frac{3PR^2}{4\pi h^3 G}\left(\frac{1-v}{2}\right) . \tag{55}$$

Taking square root of the product of both maximum deflections leads to

$$w_{\max} = \frac{3PR^2}{4\pi h^3\sqrt{EG}}(1-v)\sqrt{\frac{1+v}{2}} . \tag{56}$$

Introducing the dimensionless parameters

$$w_{\max}^{(E**)} = \frac{4\pi h^3 w_{\max} E}{3PR^2} , \tag{57}$$

$$w_{\max}^{(G**)} = \frac{4\pi h^3 w_{\max} G}{3PR^2} \tag{58}$$

and

$$w_{\max}^{(\sqrt{EG}**)} = \frac{4\pi h^3 w_{\max}\sqrt{EG}}{3PR^2} \tag{59}$$

the following dimensionless maximum deflections

$$w_{\max}^{(E**)} = 1-v^2 , \tag{60}$$

$$w_{\max}^{(G**)} = \frac{1-v}{2} \tag{61}$$

and

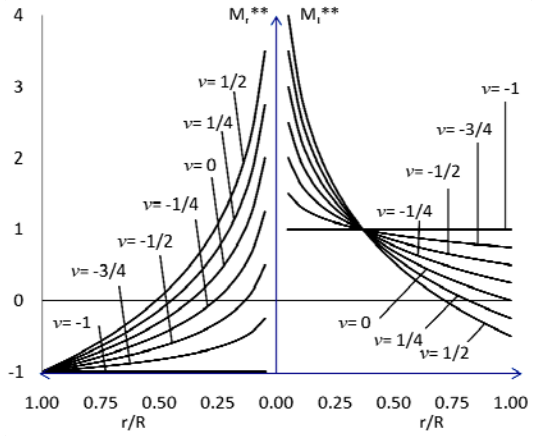
$$w_{\max}^{(\sqrt{EG}**)} = (1-v)\sqrt{\left(\frac{1+v}{2}\right)} \tag{62}$$

are obtained for quantifying the maximum plate deflection on the basis of constant Young's modulus, constant shear modulus, and constant product of both moduli, as the plate material changes in its Poisson's ratio. By the choice of dimensionless parameters shown in Eqs. (57) to (59), the dimensionless maximum deflections for central point load with fully-clamped edge described by Eqs. (60) to (62) are similar to those under uniform load with similar boundary condition, *i.e.* Eqs. (29) to (31) respectively.

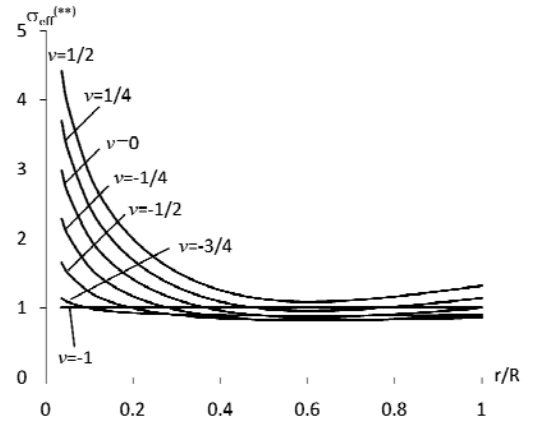
Figures 5(a) and 5(b) demonstrate the plots of dimensionless bending moments and dimensionless effective stress versus dimensionless radius for central point-loaded circular plates with fully-clamped edge, while Fig. 5(c) describe the change in the dimensionless maximum deflection with auxeticity of the plate material.

A well-known feature in a circular plate loaded at the center is the high bending moment at the loading point, as shown in Fig. 5(a). An exception is found in the case of auxetic plate with $v=-1$, which gives a constant dimensionless bending moment of $\left|M_r^{**}\right| = \left|M_t^{**}\right| = 1$ throughout the entire plate. In the range $e^{-4/3} \le (r/R) \le 1$, the dimensionless radial bending moment is bounded within $-1 \le M_r^{**} \le 1$ or $0 \le |M_r^{**}| \le 1$ for $-1 \le v \le 0.5$, while in the range $e^{-1} \le (r/R) \le 1$, the dimensionless tangential bending moment is bounded within $-1 \le M_t^{**} \le 1$ or $0 \le |M_t^{**}| \le 1$ for $-1 \le v \le 0.5$. These bounds imply non-optimal condition when the plate material possess Poisson's ratio of $v=-1$. However, $M_t^{**} > 1$ and $M_t^{**} > M_r^{**}$ for $0 \le (r/R) < e^{-1}$ such that increasing Poisson's ratio is followed by increasing dimensionless tangential bending moment. The region of maximum bending stress is thus determined at this region, thereby suggesting the suitability of limiting Poisson's ratio of $v=-1$ for a fully-clamped isotropic circular plate under concentrated lateral load at the center on the basis of bending moment distribution for the entire plate. Similarly, Fig. 5(b) shows that the effective stress is highest at the loading point, and that increasing auxeticity is useful for reducing the effective stress. Figure 5(c) reveals that reducing the Poisson's ratio of the plate material into the auxetic range is beneficial if the Young's modulus or the product of Young's modulus and shear modulus are kept constant, but not so if the reduction of Poisson's ratio occurs at constant shear modulus. In other words, the reduction of Poisson's ratio at constant Young's modulus leads to lower bending moment, lower effective stress and lower deformation especially at the plate center.

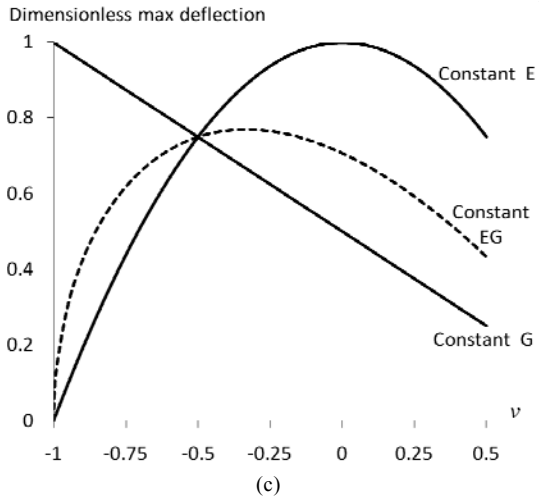
https://doi.org/10.1017/jmech.2012.113 Published online by Cambridge University Press



(a)



(b)



(c)

Fig. 5 A fully-clamped circular plate under central concentrated load: (a) dimensionless bending moment distributions, (b) dimensionless effective stress distributions, and (c) dimensionless maximum deflection

Since Eqs. (46) or (48) are not suitable for describing the bending moment, and hence the bending stress, as $r \to 0$, the following equation is herein considered for quantifying the maximum tensile stress at $r = 0$ based on theory of elasticity [49]

$$\sigma_{max} = \frac{P}{h^2}(1+\nu)\left(0.485\ln\left(\frac{R}{h}\right)+0.52\right). \tag{63}$$

Unlike the elementary model, Woinowsky-Krieger [49] showed that the maximum tensile stress at the bottom of the plate possesses a higher magnitude than the maximum compressive stress at the top of the plate where load is applied. Like the elementary model, the shear stresses are zero at both surfaces. This relation suggests that the maximum tensile stress at the plate center is minimized when an auxetic plate of $\nu = -1$ is used. For comparison with the case of simply-supported uniformly-loaded plate in the previous section, a change in the plate Poisson's ratio from $\nu = 1/3$ to $\nu = -1/3$ for the case of fully-clamped centrally loaded plate reduces the maximum tensile stress by 50% by using Eq. (63).

The bending moments for a circular plate with a point load P applied at the center of the plate that is simply-supported at the edge are given as [45-48]

$$\begin{Bmatrix} M_r \\ M_t \end{Bmatrix} = \frac{P}{4\pi}\begin{bmatrix} 1+\nu & 0 \\ 1+\nu & 1-\nu \end{bmatrix}\begin{Bmatrix} \ln(R/r) \\ 1 \end{Bmatrix}. \tag{64}$$

Adopting dimensionless parameters as before, we obtain

$$\begin{Bmatrix} M_r^{**} \\ M_t^{**} \end{Bmatrix} = (1+\nu)\begin{bmatrix} 1 & 0 \\ 1 & \left(\frac{1-\nu}{1+\nu}\right) \end{bmatrix}\begin{Bmatrix} \ln(R/r) \\ 1 \end{Bmatrix}. \tag{65}$$

Substituting Eq. (64) into Eq. (4) and using the dimensionless stress parameter described by Eq. (49), the effective stress of Eq. (13) can be written as

$$\sigma_{eff} = \frac{3P}{2\pi h^2}\sqrt{\left[(1+\nu)\ln\left(\frac{R}{r}\right)\right]^2 + (1-\nu^2)\ln\left(\frac{R}{r}\right) + (1-\nu)^2} \tag{66}$$

or in its dimensionless form as

$$\sigma_{eff}^{(**)} = \sqrt{\left[(1+\nu)\ln\left(\frac{R}{r}\right)\right]^2 + (1-\nu^2)\ln\left(\frac{R}{r}\right) + (1-\nu)^2}. \tag{67}$$

The plate deflection

$$w = \frac{P}{16\pi D}\left[\frac{3+\nu}{1+\nu}(R^2-r^2) + 2r^2\ln\left(\frac{r}{R}\right)\right] \tag{68}$$

is maximum at the center

$$w_{max} = \frac{PR^2}{16\pi D}\left(\frac{3+\nu}{1+\nu}\right). \tag{69}$$

Substituting the plate bending stiffness expression into the maximum plate deflection, we have

$$w_{max} = \frac{3PR^2}{4\pi h^3 E}(3+\nu)(1-\nu) \tag{70}$$

or, by using Eq. (23),

$$w_{max} = \frac{3PR^2}{4\pi h^3 G}\frac{(3+\nu)(1-\nu)}{2(1+\nu)}. \tag{71}$$

https://doi.org/10.1017/jmech.2012.113 Published online by Cambridge University Press

Taking square root of the product of both maximum deflections leads to

$$w_{\max} = \frac{3PR^2}{4\pi h^3\sqrt{EG}} \frac{(3+\nu)(1-\nu)}{\sqrt{2(1+\nu)}} . \quad (72)$$

Using the dimensionless parameters listed in Eqs. (57) to (59) the following dimensionless maximum deflections were obtained

$$w_{\max}^{(E^{**})} = (3+\nu)(1-\nu) , \quad (71)$$

$$w_{\max}^{(G^{**})} = \frac{(3+\nu)(1-\nu)}{2(1+\nu)} \quad (72)$$

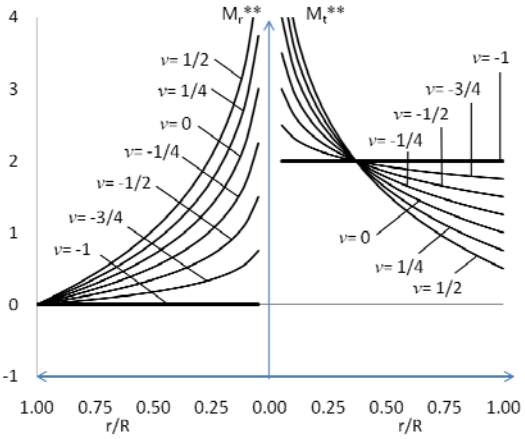
and

$$w_{\max}^{(\sqrt{EG}^{**})} = \frac{(3+\nu)(1-\nu)}{\sqrt{2(1+\nu)}} \quad (73)$$

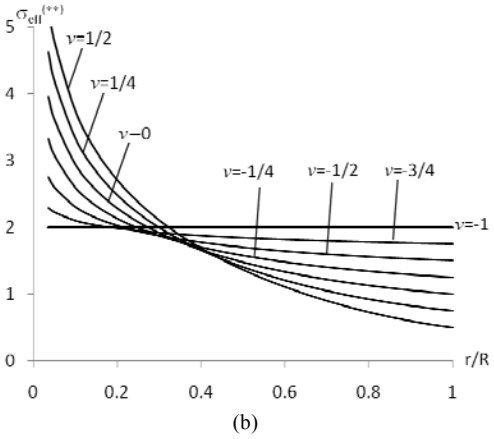
for quantifying the maximum plate deflection on the basis of constant Young's modulus, constant shear modulus, and constant product of both moduli, as the plate material changes in its Poisson's ratio.

Figures 6(a) and 6(b) show the variation of dimensionless bending moments and dimensionless effective stress with respect to the dimensionless radius for central point-loaded circular plates with simply-supported edge, while Fig. 6(c) depicts the variation in the dimensionless maximum deflection with auxeticity of the plate material.

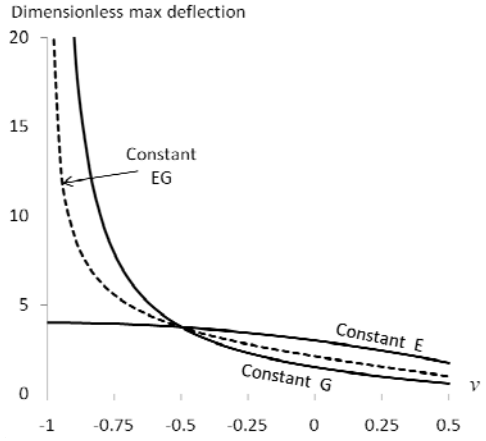
Similar to the case of clamped edge, the bending moments according to Eqs. (64) or (65) approach infinity as $r \to 0$. Unlike the case of clamped plates, Fig. 6(a) shows that the dimensionless bending moments are $M_r^{**} = 0$ and $M_t^{**} = 2$ throughout the entire plate for $\nu = -1$. In the case of dimensionless radial bending moment, $M_r^{**} \geq 0$ such that M_r^{**} decreases with increasing auxeticity and increasing radial distance. In the case of dimensionless tangential bending moment, $0.5 \leq M_t^{**} \leq 2$ within $e^{-1} \leq (r/R) < 1$ for $-1 \leq \nu \leq 0.5$. In this range, bending stress decreases with increasing Poisson's ratio. However, $M_t^{**} > 2$ for $0 \leq (r/R) < e^{-1}$ and is higher than M_r^{**} at equal radius and Poisson's ratio. Since the tangential bending stress increases with increasing Poisson's ratio for this range, the maximum bending stress is determined at this range of radius, thereby suggesting the use of $\nu = -1$ for ideal stress minimization. The use of highly auxetic material is shown in Fig. 6(b) to be useful for distributing the effective stress, as opposed to the use of conventional materials. On the other hand, the use of conventional materials tend to give lower deflection of the plate center, as shown in Fig. 6(c), in which the reduction of Poisson's ratio at constant shear modulus and at constant product of Young's and shear moduli tend to give very large deflection at the plate center. As such the use of highly auxetic plate for reducing the bending moments and effective stress can be best achieved if the reduction of the Poisson's ratio is accompanied by constant Young's modulus to limit the plate deflection.



(a)



(b)



(c)

Fig. 6 A simply-supported circular plate under central concentrated load: (a) dimensionless bending moment distributions, (b) dimensionless effective stress distributions, and (c) dimensionless maximum deflection

Due to the unsuitability of Eqs. (64) and (65) for describing the bending moment, and hence the bending stress, at the plate center, the following equation has been developed [49]

$$\sigma_{\max} = \frac{P}{h^2}\left[(1+\nu)\left(0.485\ln\left(\frac{R}{h}\right)+0.52\right)+0.48\right] . \quad (74)$$

This relation again suggests the suitability of auxetic plate with $\nu = -1$ for minimizing the bending stress at

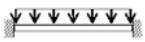
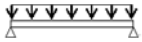
https://doi.org/10.1017/jmech.2012.113 Published online by Cambridge University Press

the center of the plate. For comparison again with the case of simply-supported uniformly-loaded plate in the previous section, a change in the plate Poisson's ratio from $v = 1/3$ to $v = -1/3$ for the case of simply-supported centrally loaded plate reduces the maximum tensile stress by between 30% and 50% based on extreme radius to thickness ratios of $(R/h) = 1$ and $(R/h) \to \infty$ respectively.

5. SUMMARY

The choice of ideal Poisson's ratio of plate material for minimizing bending stresses of plates have been considered in this paper, and quantified for a few special cases. For the bending of a flat circular plate into a spherical shell cap and in cases of concentrated load on the center of a circular plate, the use of plate material with $v = -1$ is recommended for stress minimization. In the case of uniformly loaded circular plates with simply-supported edge, the use of materials with $v = -1/3$ minimizes the bending stress by evenly redistributing the tangential bending moment. The Poisson's ratio of $v = -1/3$ is interesting as it is the threshold which the location of maximum bending stress shrifts from the plate center to the plate edge. Not all plate bending cases, however, are advantageous with the use of auxetic materials. In some cases, the maximum bending stress is independent from the Poison's ratio as in the case of uniformly loaded circular plate that is fully clamped at its edge. In other cases, neither auxetic nor conventional materials are advantageous, as in the case of bending of a plate into a cylindrical shell. There are also cases where the use of auxetic materials is discouraged, as in the bending of a plate into a saddle-like shell. A summary of load descriptions, percentage difference in maximum stress of a conventional plate ($v = 1/3$) with its auxetic counterpart ($v = -1/3$), and the optimal Poisson's ratios for stress minimization are listed in Table 1 for some special cases of plate bending. A region of dimensionless bending moments for circular plates with uniform and point loads under simply supported and clamped edges can be broadly identified as conventional and auxetic windows, as shown in Fig. 7.

Table 1 List of loadings on plates and the effect of auxeticity on bending stresses

Schematics	Load descriptions	% change in maximum stress from $v = 1/3$ to $v = -1/3$	Optimal v for stress minimization
	Bending of a plate into a saddle-like shell.	If $r_x = -2r_y$, then $\Delta_{max} = +400\%$ (Increased stresses)	If $r_x = -2r_y$, then σ_x is minimized when $v = 1/2$
	Bending of a plate into a cylindrical shell.	$\Delta\sigma_{max} = 0\%$ (No change)	$v = 0$
	Bending of a plate into a spherical shell.	$\Delta\sigma_{max} = -50\%$ (Reduced stresses)	$v = -1$
	Uniform load on fully-clamped circular plate.	$\Delta\sigma_{max} = 0\%$ (No change)	N.A.
	Uniform load on simply-supported circular plate.	$\Delta\sigma_{max} = -20\%$ (Reduced stresses)	$v = -1/3$
	Concentrated load on center of fully-clamped circular plate.	$\Delta\sigma_{max} = -50\%$ (Reduced stresses)	$v = -1$
	Concentrated load on center of simply-supported circular plate.	$\Delta\sigma_{max} \approx -40\%$ (Reduced stresses)	$v = -1$

https://doi.org/10.1017/jmech.2012.113 Published online by Cambridge University Press

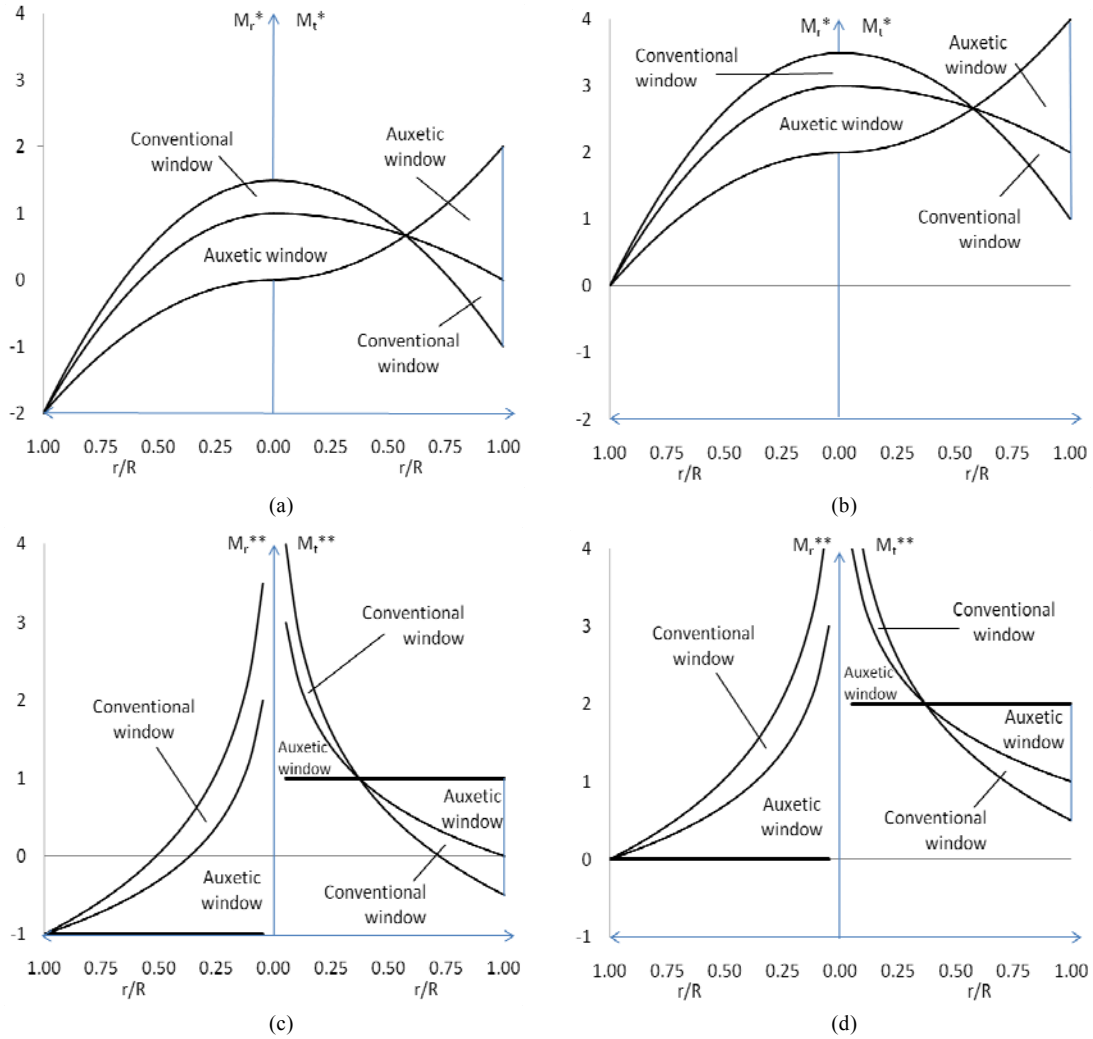


Fig. 7 Conventional and auxetic windows for (a) uniform load with clamped edge, (b) uniform load with simply-supported edge, (c) point load with clamped edge, and (d) point load with simply-supported edge on the basis of dimensionless bending moments

6. CONCLUDING REMARKS

In essence the use of auxetic materials to control the extent of bending stresses offer wider choices in the design of structural elements. This approach is comparable to two broad approaches: Structural dimensioning and materials strengthening. In structural dimensioning approach, the choice of materials is typically fixed while the structure's dimensions are sized so as to reduce the stress across wider cross-sectional area or to reduce stress intensity by removing notches and small holes. In materials strengthening approach, the structural dimensions are normally fixed due to geometrical constraints while materials of higher strength and toughness are selected to withstand high stresses. The control of Poisson's ratio is a blend of both earlier techniques, in that it redistributes stresses – akin to the dimensioning approach - so as to lower the maximum stresses while the selection of optimal Poisson's ratio is in itself a materials engineering approach. Since almost all materials possess positive Poisson's ratio, mechanical design literatures assume positive Poisson's ratio in stress analysis for design purposes. This assumption is normally valid but with increasing discovery of natural auxetic materials and synthetic auxetic materials [50-56], increased emphasis on wider range of Poisson's ratio materials, including auxetic materials, not only offers wider choice of design methodology but also provides the possibility of stronger and more durable product and structural designs. In addition, it is shown that existing design consideration is no longer applicable as a result of high level of auxeticity. For example, the maximum bending moment, and hence the maximum bending stresses, for a simply-supported uniformly loaded circular plate is known to be located at the center of the plate. This is no longer true if the plate material's Poisson's ratio is less than -1/3.

REFERENCES

1. Popereka, M. Y. A. and Balagurov, V. G., "Ferromagnetic Films Having a Negative Poisson Ratio," *Fizika Tverdogo Tela*, **11**, pp. 3507–3513 (1969).
2. Milstein, F. and Huang, K., "Existence of a Negative Poisson Ratio in FCC Crystals," *Physical Re-*

https://doi.org/10.1017/jmech.2012.113 Published online by Cambridge University Press

view B, **19**, pp. 2030–2033 (1979).
3. Wojciechowski, K. W., "Two-Dimensional Isotropic System with a Negative Poisson Ratio," *Physics Letters A*, **137**, pp. 60–64 (1989).
4. Wojciechowski, K. W. and Branka, A. C., "Negative Poisson's Ratio in Isotropic Solids," *Physical Review A*, **40**, pp. 7222–7225 (1989).
5. Lakes, R., "Foam Structures with Negative Poisson's Ratio," *Science*, **235**, pp. 1038–1040 (1987).
6. Lakes, R., "Negative Poisson's Ratio Materials," *Science*, **238**, p. 551 (1987).
7. Caddock, B. D. and Evans, K. E., "Microporous Materials with Negative Poisson's Ratios I: Microstructure and Mechanical Properties," *Journal of Physics D: Applied Physics*, **22**, pp. 1877–1882 (1989).
8. Evans, K. E. and Caddock, B. D., "Microporous Materials with Negative Poisson's Ratios II: Mechanisms And Interpretation," *Journal of Physics D: Applied Physics*, **22**, pp. 1883–1887 (1989).
9. Choi, J. B. and Lakes, R. S., "Design of a Fastener Based on Negative Poisson's Ratio Foam," *Cellular Polymers*, **10**, pp. 205–212 (1991).
10. Caddock, B. D. and Evans, K. E., "Negative Poisson Ratios and Strain-Dependent Mechanical Properties in Arterial Prostheses," *Biomaterials*, **16**, pp. 1109–1115 (1995).
11. Martz, E. O., Lakes, R. S., Goel, V. K. and Park, J. B., "Design of an Artificial Intervertebral Disc Exhibiting a Negative Poisson's Ratio," *Cellular Polymers*, **24**, pp. 127–138 (2005).
12. Dolla, W. J. S., Fricke, B. A. and Becker, B. R., "Structural and Drug Diffusion Models of Conventional and Auxetic Drug-eluting Stents," *Journal of Medical Devices*, **1**, pp.47–55 (2007).
13. Scarpa, F., "Auxetic Materials for Bioprostheses," *IEEE Signal Processing Magazine*, **25**, pp.125–126 (2008).
14. Lakes, R. S. and Lowe, A., "Negative Poisson's Ratio Foam as Seat Cushion Material," *Cellular Polymers*, **19**, pp. 157–167 (2000).
15. Wang, Y. C. and Lakes, R. S., "Analytical Parametric Analysis of the Contact Problem of Human Buttocks and Negative Poisson's Ratio Foam Cushions," *International Journal of Solids and Structures*, **39**, pp. 4825–4838 (2002).
16. Alderson, A., Rasburn, J., Ameer-Bag, S., Mullarkey, P. G., Perrie, W. and Evans, K. E., "An Auxetic Filter: A Tuneable Filter Displaying Enhanced Size Selectivity or De-fouling Properties," *Industrial & Engineering Chemistry Research*, **39**, pp. 654–655 (2000).
17. Alderson, A., Davies, P. J., Evans, K. E., Alderson, K. L. and Grima, J. N., "Modelling of the Mechanical and Mass Transport Properties of Auxetic Molecular Sieves: An Idealised Inorganic (Zeolitic) Host-Guest System," *Molecular Simulation*, **31**, pp. 889–896 (2005).
18. Alderson, A., Davies, P. J., Williams, M. R., Evans, K. E., Alderson, K. L. and Grima, J. N., "Modelling of the Mechanical and Mass Transport Properties of Auxetic Molecular Sieves: An Idealised Organic (Polymeric Honeycomb) Host-Guest System," *Molecular Simulation*, **31**, pp. 897–905 (2005).
19. Lim, T. C. and Acharya, R. U., "Performance Evaluation of Auxetic Molecular Sieves with Re-Entrant Structures," *Journal of Biomedical Nanotechnology*, **6**, pp. 718–724 (2010).
20. Scarpa, F., Giacomin, J., Zhang, Y. and Pastorino, P., "Mechanical Performance of Auxetic Polyurethane Foam for Antivibration Glove Applications," *Cellular Polymers*, **24**, pp. 253–268 (2005).
21. Alderson, A. and Alderson, K., "Expanding Materials and Application: Exploiting Auxetic Textiles," *Technical Textiles International*, **14**, pp. 29–34 (2005).
22. Park, K. O., Choi, J. B., Lee, S. J., Choi, H. H. and Kim, J. K., "Polyurethane Foam with Negative Poisson's Ratio for Diabetic Shoe," *Key Engineering Materials*, **288&289**, pp. 677–680 (2005).
23. Ellul, B., Muscat, M. and Grima, J. N., "On the Effect of the Poisson's Ratio (Positive and Negative) on the Stability of Pressure Vessel Heads," *Physics Status Solidi B*, **246**, pp. 2025–2032 (2009).
24. Salit, V. and Weller, T., "On the Feasibility of Introducing Auxetic Behavior Into Thin Walled Structures," *Acta Materialia*, **57**, pp. 125–135 (2009).
25. Whitty, J. P. M., Henderson, B., Myler, P. and Chirwa, C., "Crash Performance of Cellular Foams with Reduced Relative Density Part 2: Rib Deletion," *International Journal of Crashworthiness*, **12**, pp. 689–698 (2007).
26. Park, K. O., Choi, J. B., Park, J. C., Park, D. J. and Kim, J. K., "An Improvement in Shock Absorbing Behavior of Polyurethane Foam with a Negative Poisson Effect," *Key Engineering Materials*, **342**, pp. 845–848 (2007).
27. Alderson, K. L., Weber, R. S. and Evans, K. E., "Microstructural Evolution in the Processing of Auxetic Microporous Polymers," *Physica Status Solidi B*, **244**, pp. 828–841 (2007).
28. Grima, J. N. and Evans, K. E., "Auxetic Behavior from Rotating Squares," *Journal of Materials Science Letters*, **19**, pp. 1563–1565 (2000).
29. Grima, J. N. and Evans, K. E., "Auxetic Behavior from Rotating Triangles," *Journal of Materials Science Letters*, **41**, pp. 3193–3196 (2006).
30. Grima, J. N., Zammit, V., Gatt, R., Alderson, A. and Evans, K. E., "Auxetic Behaviour from Rotating Semi-Rigid Units," *Physica Status Solidi B*, **244**, pp. 866–882 (2007).

https://doi.org/10.1017/jmech.2012.113 Published online by Cambridge University Press

31. Liu, Y. and Hu, H., "A Review on Auxetic Structures and Polymeric Materials," *Scientific Research Essays*, **5**, pp. 1052–1063 (2010).
32. Bianchi, M., Scarpa, F., Banse, M. and Smith, C. W., "Novel Generation of Auxetic Open Cell Foams for Curved And Arbitrary Shapes," *Acta Materialia*, **59**, pp. 686–691 (2011).
33. Gaspar, N., Smith, C. W., Alderson, A., Grima, J. N. and Evans, K. E., "A Generalised Three-Dimensional Tethered-Nodule Model for Auxetic Materials," *Journal of Materials Science*, **46**, pp. 372–384 (2011).
34. Grima, J. N., Manicaro, E. and Attard, D., "Auxetic Behaviour from Connected Different-Sized Squares and Rectangles," *Proceedings of the Royal Society A*, **467**, pp. 439–458 (2011).
35. Taylor, C. M., Smith, C. W., Miller, W. and Evans, K. E., "The Effects of Hierarchy on the In-Plane Elastic Properties of Honeycombs," *International Journal of Solids and Structures*, **48**, pp. 1330–1339 (2011).
36. Lim, T. C. and Acharya, R. U., "An Hexagonal Array of Fourfold Interconnected Hexagonal Nodules for Modeling Auxetic Microporous Polymers: A Comparison of 2D and 3D Models," *Journal of Materials Science*, **44**, pp. 4491–4494 (2009).
37. Bianchi, M., Scarpa, F., Smith, C. W. and Whittell, G. R., "Physical and Thermal Effects on the Shape Memory Behaviour of Auxetic Open Cell Foams," *Journal of Materials Science*, **45**, pp. 341–347 (2010).
38. Scarpa, F. and Tomlinson, G., "Theoretical Characteristics of the Vibration of Sandwich Plates with In-Plane Negative Poisson's Ratio Values," *Journal of Sound and Vibration*, **230**, pp. 45–67 (2000).
39. Ruzzene, M., Mazzarella, L., Tsopelas, P. and Scarpa, F., "Wave Propagation in Sandwich Plates with Periodic Auxetic Core," *Journal of Intelligent Material Systems and Structures*, **13**, pp. 587–597 (2002).
40. Bullar, S. K., Wegner, J. L., and Mioduchowski, A., "Auxetic Behavior of a Thermoelastic Layered Plate," *Journal of Engineering Technology Research*, **2**, pp. 161–167 (2010).
41. Bullar, S. K., Wegner, J. L., and Mioduchowski, A., "Strain Energy Distribution in an Auxetic Plate with a Crack," *Journal of Engineering Technology Research*, **2**, pp. 118–126 (2010).
42. Strek, T., Maruszewski, B., Narojczyk, J. and Wojciechowski, K. W., "Finite Element Analysis of Auxetic Plate Deformation," *Journal of Non-Crystalline Solids,* **354**, pp. 4475–4480 (2008).
43. Poźniak, A. A., Kamiński, H., Kędziora, P., Maruszewski, B., Stręk, T. and Wojciechowski, K. W., "Anomalous Deformation of Constrained Auxetic Square," *Reviews on Advanced Materials Science*, **23**, pp. 169–174 (2010).
44. Kolat, P., Maruszewski, B. M. and Wojciechowski, K. W., "Solitary Waves in Auxetic Plates," *Journal of Non-Crystalline Solids*, **356**, pp. 2001–2009 (2010).
45. Timoshenko, S. P. and Woinowsky-Krieger, S., *Theory of Plates and Shells*, 2nd Ed., McGraw-Hill, New York, Chap. 5 (1964).
46. Ugural, A. C., *Stresses in Plates and Shells*, 2nd Ed., McGraw-Hill, New York (1998).
47. Ventsel, E. and Krauthammer, T., *Thin Plates and Shells: Theory*, *Analysis and Applications*, Marcel Dekker, New York (2001).
48. Reddy, J. N., *Theory and Analysis of Elastic Plates and Shells*, 2nd Ed., CRC Press, Boca Raton (2006).
49. Woinowsky-Krieger, S., "Der Spannungszustand in Dicken Elastischen Platen II," *Ingenieur Archiv*, **4**, pp. 305–331. (In German for: "The State of Stress in Thick Elastic Plates - Part 2") (1933).
50. Almgren, R. F., "An Isotropic Three Dimensional Structure with Poisson's Ratio = –1," *Journal of Elasticity*, **15**, pp. 427–430 (1985).
51. Haeri, A. Y., Weidner, D. J. and Parise, J. B., "Elasticity of Alpha-Cristobalite: A Silicon Dioxide with a Negative Poisson's Ratio," *Science*, **257**, pp. 650–652 (1992).
52. Warren, T. L., "Negative Poisson Ratio in a Transversely Isotropic Foam Structure," *Journal of Applied Physics*, **67**, pp. 7591–7594 (1990).
53. Ugbolue, S. C., Kim, Y. K., Warner, S. B., Fan, Q., Yang, C. L., Kyzymchuk, O., Feng, Y. and Lord, J., "The Formation and Performance of Auxetic Textiles. Part II: Geometry and Structural Properties," *Journal of the Textile Institute*, **102**, pp. 424–433 (2011).
54. Sloan, M. R., Wright, J. R. and Evans, K. E., "The Helical Auxetic Yarn – A Novel Structure for Composites and Textiles; Geometry, Manufacture and Mechanical Properties," *Mechanical Materials*, **43**, pp. 476–486 (2011).
55. Lira, C., Scarpa, F. and Rajasekaran, R., "A Gradient Cellular Core for Aeroengine Fan Blades Based on Auxetic Configurations" *Journal of Intelligent Material Systems and Structures*, **22**, pp. 907–917 (2011).
56. Dos Reis, F. and Ganghoffer, J. F., "Equivalent Mechanical Properties of Auxetic Lattices from Discrete Homogenization," *Computational Materials Science*, **51**, pp. 314–321 (2012).

(Manuscript received December 15, 2011,
accepted for publication May 21, 2012.)

https://doi.org/10.1017/jmech.2012.113 Published online by Cambridge University Press